JOURNAL OF APPLIED ELECTROCHEMISTRY 22 (1992) 950–958

Mass transfer in an electrochemical reactor with two interacting jets

Y. OREN*, M. ABDA

Department of Chemistry, Nuclear Research Center, Negev, P.O. Box 9001, Beer-Sheva 84190, Israel

A. TAMIR

Department of Chemical Engineering, Ben-Gurion University of the Negev, P.O. Box 653, Beer-Sheva 84105, Israel

Received 11 June 1991; revised 6 March 1992; accepted 6 March 1992

An electrochemical reactor operated with two identical solution streams injected in opposite directions on the same axis, and leaving it at a normal direction was studied by measuring local and global mass transfer coefficients and visualization of solution flow patterns. This flow configuration was compared to a case where a single stream enters the reactor and leaves it on the same axis. It was found that only the data obtained for the single stream mode can be correlated by the Chilton–Colburn relation, indicating a near laminar boundary layer flow. Global mass transfer coefficients for the single stream mode were found to be slightly higher than those for the interacting jets mode. However, when comparing the two modes by taking into account the dimensionless ratio of the mass transfer coefficient (*Sh*) to the energy consumption (*Eu*), it was found that the interacting jets (IJ) mode exhibits a better performance as compared to the single stream mode. The superiority of the IJ mode increases with increasing Reynold's number (*Re*).

Nomenclature

A, B	adjustable parameters
b	half width of channel
C	electrolyte ion concentration
d	inlet pipe diameter
d'	microelectrode diameter
D	diffusion coefficient
$\bar{D}_{max}$	maximum value of mean deviation
E	pumping energy
Eu	Euler number
F	Faraday number
i	current to a single microelectrode on an active wall
i'	current to a single microelectrode in an inert wall
I	global diffusion current
k	mass transfer coefficient to a single microelectrode in an active wall
k'	mass transfer coefficient to a single microelectrode in an inert wall
K	global mass transfer coefficient
Q	volumetric flow rate
Q_T	total volumetric flow rate
R	radius of the electrochemical reactor
Re	Reynolds number
s	surface area of a microelectrode
S	surface area of the working electrode
Sc	Schmidt number
Sh	Sherwood number
V_x	axial flow velocity along x-axis
V_∞	flow velocity at large distance from the leading edge
V	mean flow velocity
x	axis tangential to the surface
y	axis normal to the surface
z	number of electrons transferred in the reaction ($z = 1$ in the present case)

Greek letters

μ	viscosity
ρ	specific gravity
ν	kinematic viscosity (μ/ρ)
ΔP	pressure drop across the reactor
ΔV	voltage drop across the reactor

Abbreviations

ST	single stream
IJ	interacting jets

1. Introduction

Enhancement of mass and heat transfer is essential for the improvement of the space-time yield of chemical and electrochemical reactors. Numerous studies have been devoted to the investigation of new methods for the intensification of electrode reactions. These studies can be roughly divided into two classes: (a) those utilizing various types of high surface area electrodes

* To whom all correspondence should be addressed

0021-891X/92

and, (b) those in which the solution flow regime within the reactor is modified.

The flow modification approach, into which the present study fits, is aimed at studying novel techniques for reducing the thickness of the concentration boundary layer at the solution/electrode interface by, for example, promoting turbulent flow and improving current distribution in large scale electrochemical reactors.

One way of improving mass transfer is by use of turbulence promoters. This can be done either by roughening the electrode surface as demonstrated by Gabe and Makanjuola [1] on a roughened rotating cylinder electrode, or by implanting promoters of various shapes within the reactor as shown by Stork and Coeuret [2, 3]. Wragg and Leontaritis [4] showed that a baffled parallel plate electrochemical reactor generates higher mass transfer coefficients which were more evenly distributed as compared to an unbaffled reactor.

In the present study a new electrochemical reactor flow configuration is investigated. This involves the interaction over a flat electrode, of two identical electrolyte jets entering a cell in opposite directions and leaving in a direction perpendicular to that of the entering flow, as illustrated in Fig. 1a and b.

The interacting jets concept (often termed 'impinging streams' [5]) has been proved efficient in the enhancement of mass transfer in various operations [6, 7]. In these systems, the interaction of impinging jets composed of at least two phases (such as solid particles and liquid or gas, gas bubbles and liquid etc.) results in an oscillatory movement and increased relative velocities within the impingement zone and, therefore, a significant reduction of the hydrodynamic boundary layer thickness occurs.

The case where two identical single phase fluid jets collide was also investigated. Kind and Suthanthiran [8] studied the collision of two air streams over a flat wall and determined velocity distribution, longitudinal turbulence and static pressure. It was found that the static pressure in the interaction region between the jets is larger than the ambient static pressure. As a result, a stagnant separation 'bubble' exists in the collision region. Denschhikov *et al.* [9], reached a similar conclusion with two identical submerged jets in water in an effort to model the origin of hurricane storms. They showed that the collision of the two jets is associated with retardation of the liquid, resulting in the existence of a region of increased pressure. It was also found that under some conditions the interaction between the jets is oscillatory in character. Becker and Booth [10] studied the extent of mixing in the impinging zone of two identical free jets.

The present study is aimed at characterizing the interacting jets (IJ) electrochemical reactor specified above, with respect to local and global mass transfer coefficients, static pressure and flow pattern distribution. The results attained with this flow configuration are compared to a conventional case where only a single stream (ST) enters the same reactor as described in Figure 1b.

2. Experimental details

The experimental setup is described in detail elsewhere [11]; the basic elements are given in Fig. 1a to c. The circular reactor was made of Plexiglass and was 0.07 m in diameter and 0.012 m high. It had five openings: two pairs, with diameters of 3, 5 and 8×10^{-3} m located on two perpendicular axes and the fifth was for connecting a standard calomel electrode as reference. The working and counter electrodes served as the bases of the cell. The working electrode was made of 10^{-4} m thick platinum foil glued with epoxy resin under high pressure to a copper disc, 2×10^{-3} m thick. Thirty three microelectrodes made of platinum wire, 7.5×10^{-4} m in diameter were installed at distances of 7×10^{-3} m apart on the surface of the working electrode. They were electrically isolated from the main working electrode surface by Teflon tubing and were affixed to the electrode base by an epoxy resin.

The microelectrodes in the arrangement shown in Fig. 1c allowed a detailed mapping of the mass transfer coefficients across the working electrode surface. Following the method and terminology of Nanzer and Coeuret [13], two types of measurements were performed: (a) *Active wall* measurements where both the microelectrodes and the entire working electrode were electrochemically active; (b) *Inert wall* measurements where only the microelectrodes were active.

A solution of potassium ferricyanide (2.5×10^{-3}–15×10^{-3}) M, potassium ferrocyanide (2.5×10^{-2}–15×10^{-2}) M and NaOH 0.5 M as a supporting electrolyte was used. It was maintained at 30°C and circulated by a centrifugal pump through the reactor. The physical properties of this solution are noted elsewhere [13].

Local and global mass transfer coefficients were obtained by measuring the limiting diffusion current for ferricyanide ion reduction. The results reported below represent the mean value of five measurements with a standard deviation of $\pm 3\%$.

The reactor was operated in two flow modes, viz. interacting jets and a single stream as shown in Fig. 1b.

In order to perform the flow pattern visualization, water was used and white alumina particles, 10^{-3} m in diameter, were pulse injected into the flow. The bottom electrode was replaced by a black PVC plate which served as a background for the tracer particles and the top electrode, by a circular glass window which allowed observation and photography of the alumina particle trajectories.

In order to measure the static pressure distribution within the cell, a disc on which nine glass tubes, each 1.5 m long and 3×10^{-3} in diameter were installed in the EN and EX axes (as shown in Fig. 1c), replaced

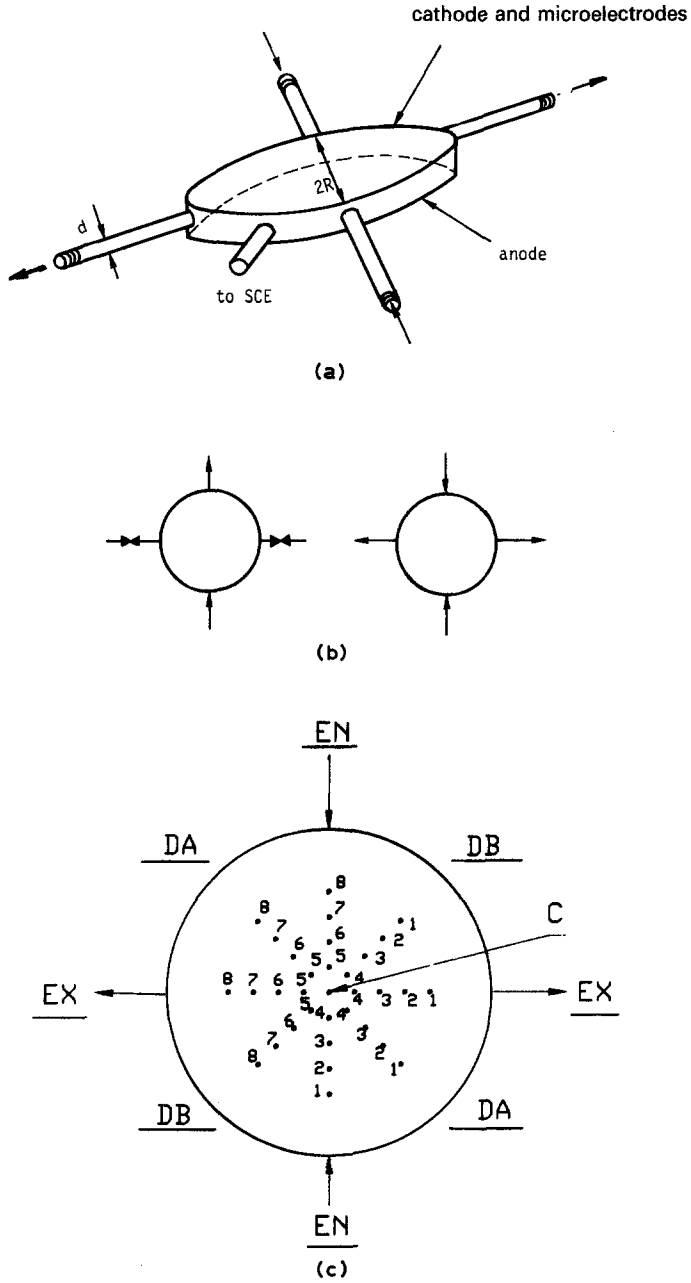

Fig. 1. Basic elements of the electrochemical cell: (a) Three dimensional layout; (b) Single stream (left) and interacting jets (right) flow configurations; (c) Microelectrode layout and axis designation.

the top electrode. The same glass tubes were also installed at the inlet and outlet of the reactor.

3. Results and discussion

Mass transfer to the working electrode under diffusion controlled conditions is governed mainly by the flow field within the reactor. Flow configuration in the reactor in study is complex both in the IJ and the ST flow modes due to secondary collisions with the walls which results in a converging–diverging flow character. This situation is close to reality because no reactor is infinite and collisions with the walls always affect to some extent the internal flow pattern. In order to follow the complex flow pattern within the reactor, flow visualization supplemented by local static pressure measurements were carried out. The data obtained from these experiments served for substantiating the mass transfer coefficient distribution patterns measured under the two flow regimes. Finally, an analysis of the behaviour of local and global mass transfer coefficients was carried out based on various hydrodynamic criteria.

3.1. *Flow visualization*

Figure 2 depicts stream lines of the flow within the reactor for IJ and ST modes for three inlet diameters. As can be seen, with the ST mode, the stream line contour is generally independent of the inlet diameter. The entering jet penetrates into the water filling the reactor, part of it leaves undisturbed while the other part collides with the walls, changes direction and creates eddies on both sides of the inlet–outlet axis.

In contrast to the behaviour in the ST mode, the stream line contours observed in the IJ mode strongly

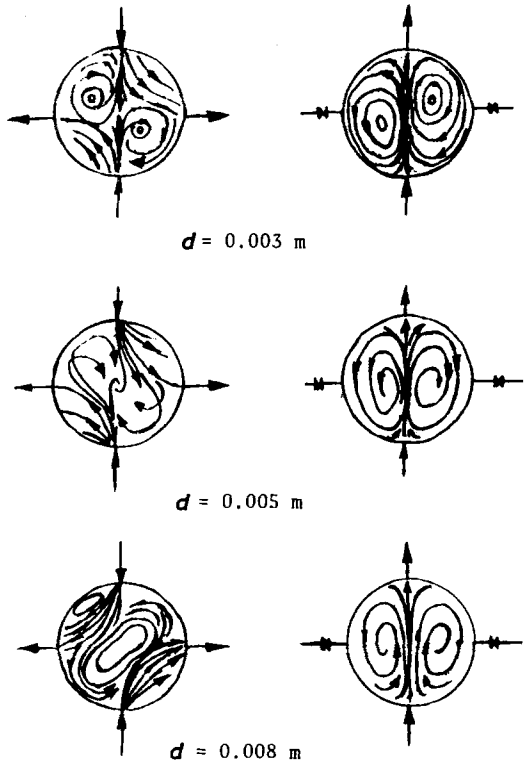

Fig. 2. Typical flow tracks plotted from photographs taken in the flow visualization experiments for several inlet opening diameters.

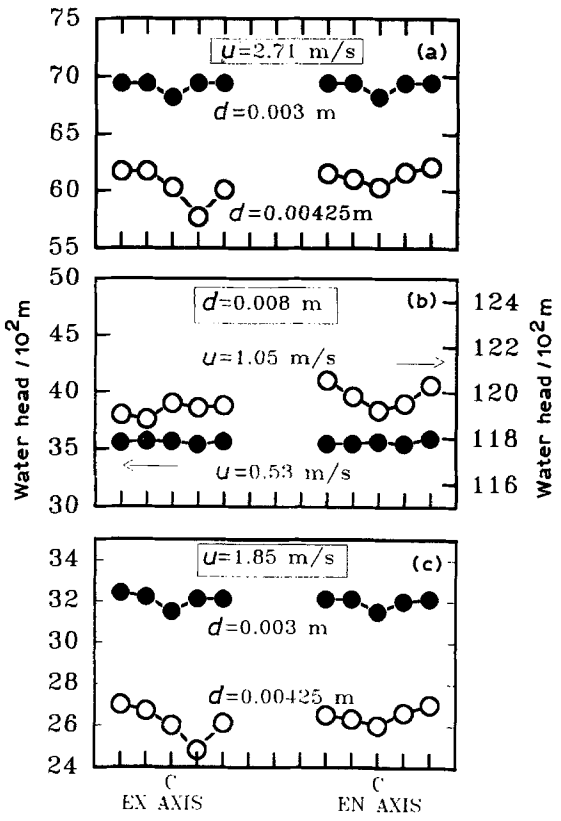

Fig. 3. Water head distribution in the cell: (a) $Q_T = 3.86 \times 10^{-5}\,m^3\,s^{-1}$; (b) $Q_T = 5.29 = 10^{-5}\,m^3\,s^{-1}$; (c) $Q_T = 2.64 \times 10^{-5}\,m^3\,s^{-1}$; (○) ST, (●) IJ.

depend on the inlet diameter: For $d = 0.003$ m, the streams interact close to the centre of the reactor and change direction towards both outlets: For $d = 0.005$ m the stream lines deflect towards the outlets before they reach the centre of the reactor. Some turbulence also occurs, but the eddies formed are less pronounced as with the ST mode. For $d = 0.008$ m the deflection of the entering jets towards the outlets become more significant although there are still some peripheral eddies which become weaker while approaching the central zone. As shown later for the IJ mode, flow velocities in this zone are the lowest compared to those in other regions of the reactor.

The fact that each entering jet is deflected closer to the entrance as the inlet diameter increases can be explained as follows. By increasing d, the velocity of the impinging jets (at a constant flow rate) becomes lower and hence the momentum of the liquid also decreases. Consequently, the increasing pressure head towards the centre (Fig. 3) affects the jets more intensively, resulting in their smaller penetration depth towards the reactor centre. It should be noted that stream deflection of the same kind was also observed by Denshchikov *et al.* [9].

The observations in Fig. 2 may be summarized as follows: in the ST mode the main flow is maintained at the central region of the cell, namely, along the inlet–outlet axis. This is also accompanied by eddy vortices located on both sides of the main flow. This pattern is independent of the inlet diameter. On the other hand, the flow pattern obtained in the IJ mode is strongly dependent on the inlet diameter. As the inlet diameter increases, that region within which the fluid velocity is smaller with respect to other (peripheral) regions due to the impingement, occupies an increasing portion of the reactor centre.

3.2. *Pressure distribution within the reactor*

In Fig. 3, local static pressures represented by their corresponding water heads measured under various conditions along two axes for the IJ and ST modes, are depicted. According to the Bernoulli equation, these heads are inversely proportional to the square of the local fluid velocities.

The conclusions from these measurements are as follows: (i) In the IJ mode, the pressures are higher than for the ST mode for identical values of inlet velocity and flow rate (Fig. 3a and c); (ii) Pressures are higher for the ST mode when total flow rate and inlet diameter are identical for both flow configurations (Fig. 3b); (iii) In both flow configurations, the lowest pressure in most cases is in the centre of the reactor.

The above observations indicate that for the ST mode, fluid velocity in the centre is the largest. On the other hand, in the IJ mode, the pressure in the centre increases with respect to the periphery as the inlet diameter increases. The implications are that with increasing the inlet diameter, the region where the two streams interact, becomes larger. Within this region, the fluid velocity decreases with respect to the periphery. As will be shown later these changes in the solution velocity strongly influence mass transfer coefficient distribution within the reactor.

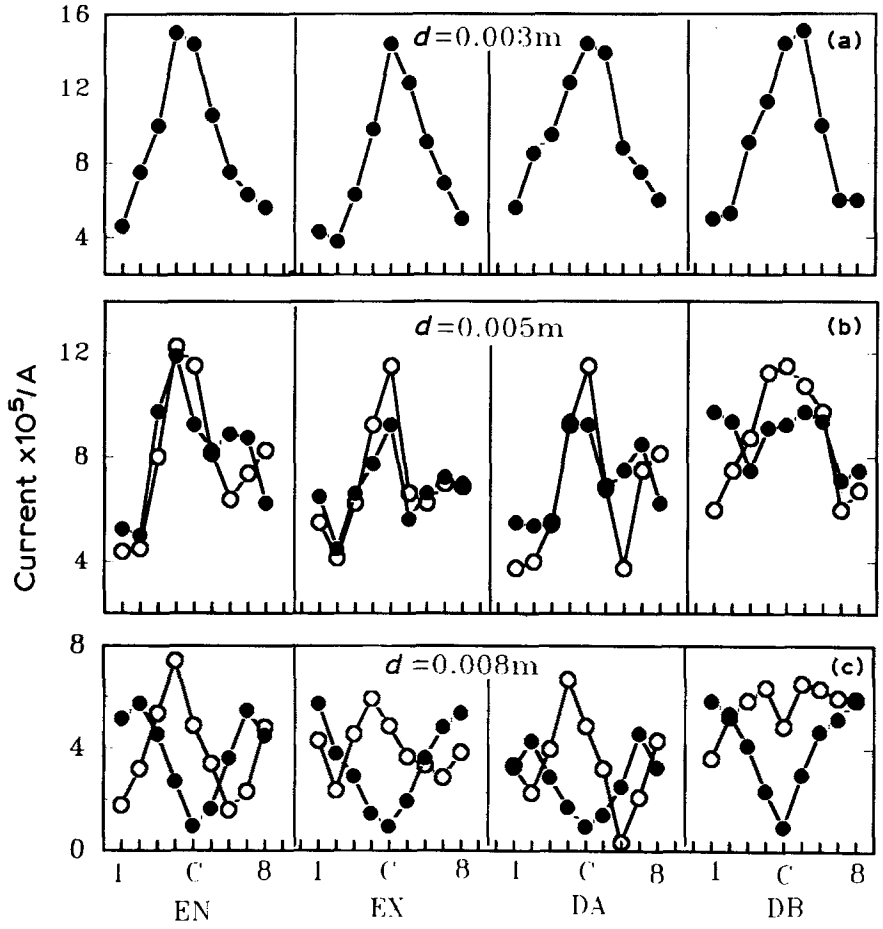

Fig. 4. Diffusion current distribution along the various axis: (○) ST; (●) IJ. Flow velocities (in $m\,s^{-1}$): (a) ● – 1.79; (b) ○ – 2.28, ● – 1.14; (c) ○ – 1.05, ● – 1.14.

3.3. *Diffusion current distribution*

Figure 4 shows the distribution of the local diffusion currents under active wall conditions along the different axes for the IJ and ST flow modes and several inlet diameters.

It is clear from the figure that diffusion current distribution strongly depend on the flow configuration as well as on the incoming flow velocity. The major feature of the diffusion currents in the ST mode for $d = 0.005$ and 0.008 m is the maximum value in the centre of the reactor following a decrease towards the walls and a rise close to them. This behaviour is in agreement with the flow visualization and the pressure distribution experiments which indicate the existence of higher flow velocities in the vicinity of the centre of the reactor. Turbulence resulting from the impingement of part of the flow on the walls is responsible for the diffusion current rise in this region.

The diffusion current distribution for the IJ mode is much more complex. The patterns shown in Fig. 4 reveal a gradual change from a symmetrical shape with a *maximum* at the centre for $d = 0.003$ m to a nearly symmetrical pattern with a *minimum* at the centre for $d = 0.008$ m for all the axes. The completely non symmetrical patterns obtained with $d = 0.005$ m, presents a transition stage between the two states. This behaviour is, again, in complete agreement with the results obtained from the pressure distribution and flow visualization measurements which indicate the existence of a zone at the centre of the cell where the fluid velocity is the highest for the smaller inlet diameter and smallest for the larger inlet diameter.

3.4. *Local mass transfer coefficients in an active and inert surface*

The following types of mass transfer coefficients, calculated from the diffusion currents are considered below. For a single microelectrode in active wall conditions,

$$k = i/(zFsC) \tag{1}$$

and for inert wall conditions,

$$k' = i'/(zFsC) \tag{2}$$

Mass transfer for the entire electrode surface,

$$K = I/(zFSC) \tag{3}$$

Figure 5 demonstrates a typical relation between k' and k at the reactor centre for the IJ and ST flow regimes and various flow rates. It is clear from the figure that: (i) both k and k' increase with increasing the solution flow; (ii) for both flow regimes, $k' > k$; and (iii) at the same flow rate, k' is approximately the same for both flow regimes while k is larger for the IJ flow mode.

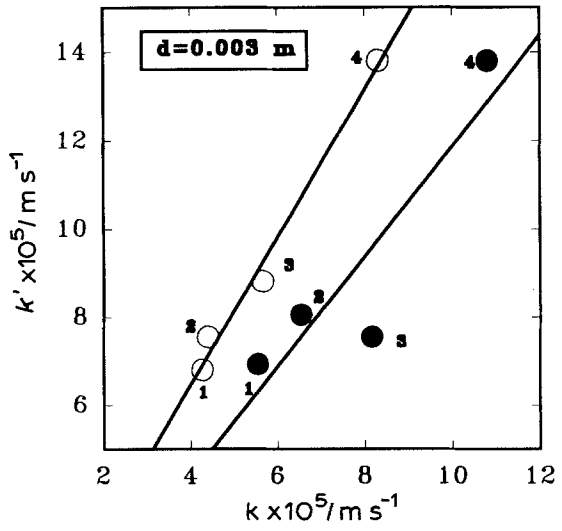

Fig. 5. Mass transfer coefficient of the central microelectrode for an inert surface as a function of the same for an active surface: (○) ST; (●) IJ; $Q_T \times 10^6$ ($m^3 s^{-1}$) = (1) 5.56, (2) 7.42, (3) 9.44, (4) 28.4.

Whereas the explanation for the first observation is straightforward, the second and the third are not self evident. The second observation may be predicted on the basis of the analysis first presented by Nanzer *et al.* [12]. According to Reiss and Hanratty [13], the mass transfer coefficient k' through an incipient differential boundary layer on a circular electrode with diameter d' located in an infinite inert surface is given by

$$k' = 0.863\, D^{2/3}\left[\left(\frac{\partial V_x}{\partial y}\right)_{y=0}\Big/ d'\right]^{1/3} \tag{4}$$

An expression for the local mass transfer coefficient under active wall conditions, k, may be deduced from the Chilton–Colburn relation [14] which reads,

$$k = \mu\left(\frac{\partial V_x}{\partial y}\right)_{y=0}\Big/ \rho V Sc^{2/3} \tag{5}$$

where V is a characteristic flow velocity.

Expressions 4 and 5 lead to the ratio,

$$\frac{k'}{k} = 0.863\left[\nu\Big/\left(\frac{\partial V_x}{\partial y}\right)_{y=0}\right]^{2/3}\frac{V}{\nu(d')^{1/3}} \tag{6}$$

The applicability of the last expression to the present case, as well as to other cases, depends on the flow distribution within the reactor since both the local normal velocity gradient and the characteristic velocity appear in this expression.

In the following discussion, simple flow models are examined with respect to the fact that $k'/k > 1$.

In the laminar boundary layer flow, the velocity profile is given by [15],

$$\frac{V_x}{V_\infty} = \frac{3}{2}\left[\frac{y}{4.64\sqrt{vx/V_\infty}}\right] - \frac{1}{2}\left[\frac{y}{4.64\sqrt{vx/V_\infty}}\right]^3 \tag{7}$$

Taking $V = V_\infty$, it is seen, from equations 6 and 7, that

$$\frac{k'}{k} = 1.832\left(\frac{x}{d'}\right)^{1/3} \tag{8}$$

Surprisingly, k'/k is independent of the flow rate.

The condition for $k'/k > 1$ for the boundary layer flow is therefore given by

$$\frac{x}{d'} > 0.163 \tag{9}$$

The second case corresponds to a flow in a rectangular channel with a well developed flow regime. The longitudinal velocity profile near the wall is given by

$$V_x = \left(\frac{3V}{b}\right)y \tag{10}$$

where y is the distance from the wall.

Differentiation of Equation 10 with respect to y, followed by substituting into Equation 6, gives

$$\frac{k'}{k} = 0.2075\left(\frac{b}{d'}\right)^{1/3} Re^{1/3} \tag{11}$$

where

$$Re = \frac{8bV}{\nu} \tag{12}$$

The condition $k'/k > 1$ is fulfilled in this case by

$$\left(\frac{b}{d}\right)Re > 111.93 \tag{13}$$

The following considerations are made in order to examine expression 9 with respect to the present case. If the performance of an ST reactor is compared to that of an IJ reactor *on the basis of identical total flow rates*, then $V_{ST} = 2V_{IJ}$. Assuming a boundary layer flow within the reactor and recalling that under these conditions, $K \propto V_\infty^{1/2}$, the following relation is obtained:

$$\frac{K_{ST}}{K_{IJ}} = \left(\frac{V_{ST}}{V_{IJ}}\right)^{1/2} = \sqrt{2} = 1.414 \tag{14}$$

Based on the values of K presented in Fig. 6, which shows the total mass transfer coefficients as calculated from Equation 3, it can be shown that the mean value of K_{ST}/K_{IJ} calculated under the above conditions is 1.36 ± 0.13 which deviates by 4% from the value predicted above. The implication is that the boundary layer theory as expressed above is relevant in the present case. Thus, applying $d' = 7.5 \times 10^{-4}$ m and $x = 7 \times 10^{-2}$ m for the microelectrode and the reactor diameters, respectively, to Equation 9 shows that the condition $k'/k > 1$ is always satisfied.

Condition 13 will be now examined. For the minimum flow rate of $5 \times 10^{-6}\ m^3 s^{-1}$, the mean velocity through the largest cross section of the reactor (i.e. 0.07×0.012 m) is $6 \times 10^{-3}\ m s^{-1}$. This yields $Re = 34$. Substituting $b = 0.07$ m and the values for d' and Re in expression 13, yields $3173 > 111.93$ which indicates that $k'/k > 1$.

The ratio $k'/k > 1$ may also be explained qualitatively as follows. When the entire electrode is electrically active, the reduction process takes place everywhere on the surface. Consequently, the mean local concentration of the active species decreases, leading to a lower diffusion current as compared to the case of an inert electrode.

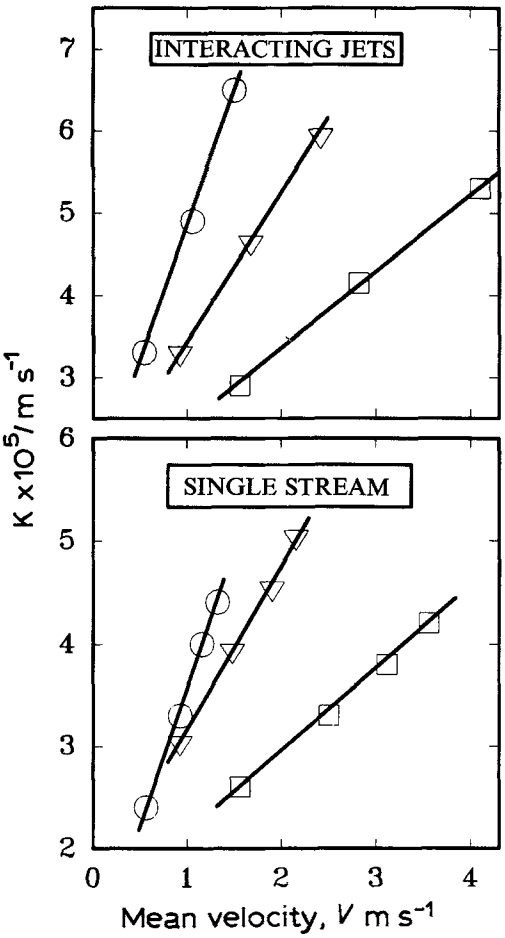

Fig. 6. Overall mass transfer coefficient as a function of the mean flow velocity at the cell inlets; $d \times 10^3$ (m) = (○) 8; (▽) 5; (□) 3.

Equation 6, obtained from Equations 4 and 5, relates k' to k. However, as emphasized above, its application is dependent on the availability of a model for the flow within the reactor. Another useful approach is to equate the terms $(\partial V_x/\partial y)_{y=0}$ from both equations. This yields,

$$\frac{k'^3}{k} = A^{-1}V \tag{15}$$

where A is a constant given by

$$A = \frac{d' Sc^{1/3}}{0.863^3 D} \tag{16}$$

Substituting the numerical values of d', Sc and D in the last expression, gives $A = 1.36 \times 10^7\ \mathrm{s\,m^{-1}}$.

As revealed by Equation 15, taking into account some characteristic value for V (for example the mean velocity at the inlet pipe), a plot of k against $(k')^3/V$ should yield a straight line with A as the slope, provided that the conditions for the Chilton–Colburn relation are satisfied. Table 1 shows values of A extracted from experimental data obtained for the ST and IJ configurations for the different axes as well as the values averaged on all the microelectrodes at each flow velocity. The following points should be emphasized: (i) the values of A in ST mode for each one of the axis, as well as for the average are, at least at the range studied and within the experimental error, independent of the flow velocity; (ii) in the IJ mode both the average and the A values in each axis are much more dispersed as the flow velocity is varied and; (iii) none of the experimental values of A are equal to the theoretical values.

Table 1. Values of $A \times 10^{-7}$ ($\mathrm{s\,m^{-1}}$) for the different axis and average at the two flow modes, various flow velocities and d = 0.008 m.

V m s^{-1}	*Axis (Fig. 1)*				
	EN	*EX*	*DA*	*DB*	*Average*
ST mode					
0.746	3.1	1.2	2.7	2.5	2.75
1.08	3.5	1.3	1.9	2.1	2.78
1.37	3.4	1.7	2.9	2.0	2.88
IJ mode					
0.86	10.6	3.8	4.3	3.9	4.69
1.12	8.3	0.5	3.5	2.1	2.64
1.35	7.4	1.3	3.2	1.8	3.07

These points indicate that the flow regime in the ST mode is closer to that required by the Chilton–Colburn analogy as compared to that in the IJ mode. The deviation of the experimental values of A in the ST mode from the theoretical may be attributed to the fact that using the inlet flow velocity for the calculation of A at the various axes is erroneous and some more realistic values should be considered.

The fact that $k_{IJ} > k_{ST}$ at the same total flow rate as shown in Fig. 5 for the central electrode, can be interpreted on the basis of the much larger effect of the IJ flow mode on mass transport in the interacting zone. However, no explanation is provided for the fact that under the same conditions, $k'_{IJ} \approx k'_{ST}$.

3.5. *A comparison between interacting jets and single stream reactors*

A comparison between an IJ and an ST reactor can be made on the basis of the following criteria: (i) the total flow rate into the reactors are identical; (ii) the total flow rates, as well as the flow velocities at the inlet pipes, are identical. This condition leads to different diameters of the inlet pipes in each reactor and; (iii) the flow velocities in the inlet pipes are identical. In this case, the total flow rate into the IJ reactor is twice that of the ST reactor.

Comparisons based on these criteria are demonstrated in Fig. 7. It is clear that all three types of comparison show that global mass transfer coefficients attained with an ST reactor are considerably higher as compared to those for the IJ reactor.

However, in comparing the two flow modes, energy consumption should also be considered. The total energy is the sum of the pumping and the electric energies, namely,

$$E = Q_T \Delta P + I \Delta V \tag{17}$$

Electrical energy consumption will be neglected in the analysis, since usually it comprises less than 10% of

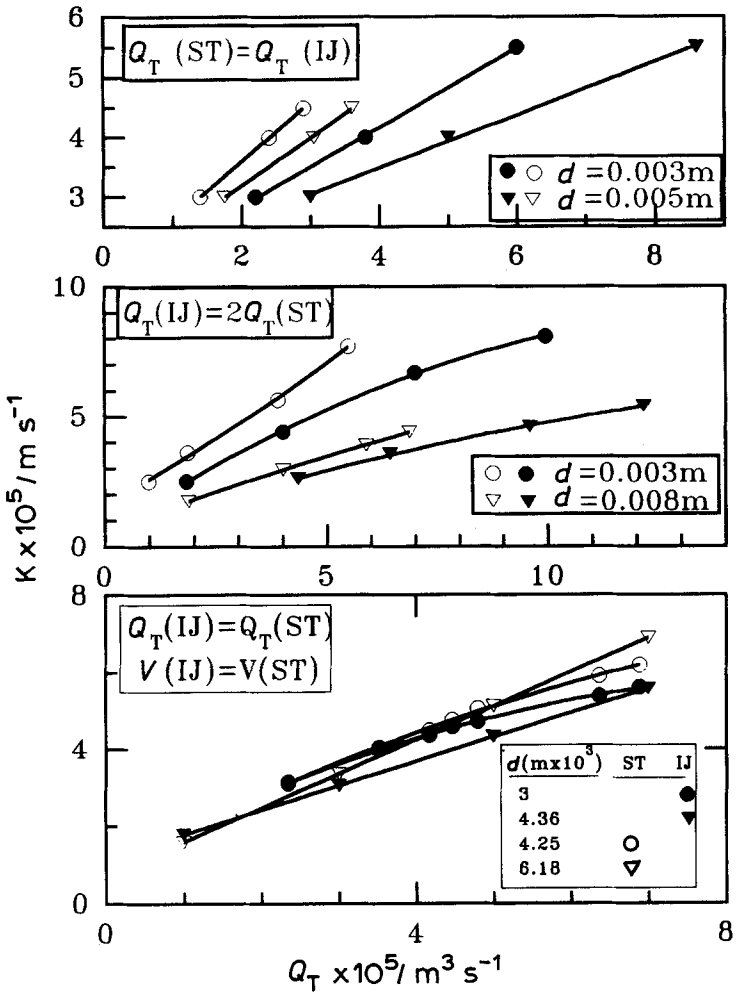

Fig. 7. Comparison between IJ and ST flow configurations at various operating conditions: (○, ▽) ST; (●, ▼) IJ.

the total energy. For the flow rate range, $23 \leqslant Q_T \times 10^6$ ($m^3 s^{-1}$) $\leqslant 69$, the following relations are obtained: For the IJ mode

$$E = -8.314 \times 10^{-4} + 32.74 Q_T \quad (18)$$

and for the ST mode,

$$E = -1.021 \times 10^{-3} + 38.53 Q_T \quad (19)$$

where E and Q_T are in kJ s^{-1} and $m^3 s^{-1}$, respectively. From the slopes of Equations 18 and 19 it may be concluded that the energy consumption for the ST mode is slightly higher than that for the IJ mode.

A more comprehensive comparison, taking into account both the mass transfer coefficients and the energy consumption, is thus required. Using the technique of dimensional analysis the following dimensionless groups are obtained:

$$\frac{Sh}{Eu} = f(Re) \quad (20)$$

where $Sh = 2K R/D$; $Eu = 2\Delta P/\rho V^2$ and $Re = dV/\nu$.

The Euler number, Eu, gives the ratio between the potential and the kinetic energies per unit volume of the solution entering the reactor. Equation 20 is in fact a convolution of the mass transfer coefficient and the pumping energy.

In Fig. 8, the ratio Sh/Eu is depicted as a function of the Reynolds number. It was obtained by operating the reactor once as an ST device with $d = 4.25 \times 10^{-3}$ m and once as an IJ reactor with $d = 3 \times 10^{-3}$ m. This provided the conditions of equal total flow rates and flow velocities at the inlets of both reactors. The major conclusion drawn from Fig. 8

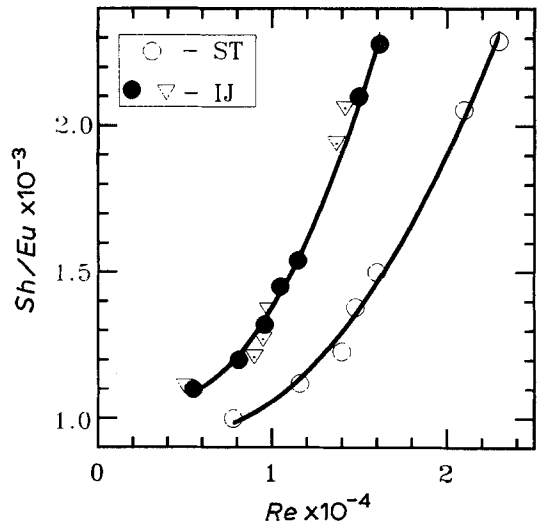

Fig. 8. Sh/Eu as a function of Re; $d \times 10^3$ (m) = (○) 4.25; (●, ▽) 3. (○, ●) measured ΔP on the reactor; (▽) extrapolated ΔP.

Table 2. Correlation parameters for Equations 21 and 22

Equation	$d \times 10^3$ m	*A*	*B*	$Re \times 10^{-3}$	
				Min.	*Max.*
IJ mode					
21*	3	721.84	6.901×10^{-5}	5.00	13.3
22	3	11.72	0.6191	4.45	23.4
22	5	12.82	0.6221	4.52	18.80
22	8	5.55	0.7191	3.86	12.20
ST mode					
21†	4.25	589.45	5.822×10^{-5}	7.70	23.0
22	3	9.73	0.6242	4.72	26.1
22	4.25	8.422	0.6352	7.79	22.9
22	5	9.225	0.6461	5.35	19.5
22	8	4.467	0.7071	3.35	12.2

* $\bar{D}_{max} = 5.7\%$;
† $\bar{D}_{max} = 3\%$;
In other cases $\bar{D}_{max} = 2\%$

is that when taking into account the ratio between the global mass transfer coefficients and the energy consumption, the IJ reactor reveals a much better performance compared with the ST reactor. These curves provide a basis for assessing one flow mode with respect to the other.

The curves in Fig. 8 can be correlated satisfactorily by the following expression,

$$Sh/Eu = A \exp(B\ Re) \quad (21)$$

Other data were correlated by the expression

$$Sh = A\ (Re)^B \quad (22)$$

where A and B are the correlation parameters given for various conditions in Table 2.

Since studying the effect of various geometrical factors was beyond the scope of the present work, Equations 21 and 22 should be used only for obtaining orders of magnitudes of the operational quantities when scale-up is considered.

4. Conclusion

This study was devoted to the characterization of a parallel plate electrochemical reactor to which two streams fed on the same axis in opposite directions, interact and leave in a perpendicular direction. This was compared to the common flow configuration where only a single stream was involved.

The flow pattern for the IJ configuration, as revealed by visualization studies, is complex due to the interaction of the two opposing streams. However, in both flow configurations secondary interactions with the reactor walls play an important role, contributing to the flow and mass transfer distribution complexity. Nevertheless, based on the well known Chilton–Colburn analysis it was concluded that averaged over the entire electrode area, the flow in the ST reactor is more uniform as compared to that in the IJ reactor where it is more turbulent in nature.

A comprehensive analysis of an electrochemical reactor should take into account both mass transfer properties and energy consumption. A concise way of doing this is to express the ratio of Sherwood to Euler numbers as a function of Reynolds number. On this basis it is shown that the IJ reactor is significantly more efficient as compared to the ST reactor.

References

[1] D. R. Gabe and P. A. Makanjuola, *J. Appl. Electrochem.* **17** (1987) 370.
[2] A. Storck and F. Coeuret, *Electrochim. Acta* **22** (1977) 1155.
[3] Y. Winograd, A. Solan and M. Toren, *Desalination* **13** (1973) 171.
[4] A. A. Wragg and A. A. Leontaritis, 'Electrochemical Cell Design and Optimization Procedures', Joint Meeting of Dechema and the Society of Chemical Industry, 24–26 September (1990), Bad-Soden, Germany.
[5] A. Tamir, 'Impinging Streams Contractors: Fundamentals and Applications', *in* 'Advances in transport processes' Vol. VIII, Elsevier, Amsterdam (1992) pp. 105–195.
[6] A. Tamir, *Chem. Eng. Prog.* **85** (1989) 53.
[7] A. Tamir and A. Kitron, *Chem. Eng. Commun.* **50** (1987) 241.
[8] R. J. Kind and K. Suthanthiran, *J. Fluid Mech.* **58** (1973) 389.
[9] V. A. Denshchikov, V. N. Kondrat'ev and A. N. Romashv, *Fluid Dynamics* **6** (1978) 924. Translated from *Izv. Akad. Nauk SSSR* **6** (1978) 165–7.
[10] H. A. Becker and B. D. Booth, *AIChE J.* **21** (5) (1975) 949.
[11] M. Abda, 'Mass transfer to a flat electrode in the impinging jets and single stream regime', M. Sc. Thesis, The Ben-Gurion University of the Negev, Beer-Sheva, Israel (1991).
[12] J. Nanzer, A. Donizeau and F. Coeuret, *J. Appl. Electrochem.* **14** (1984) 51.
[13] L. P. Reiss and T. J. Hanratty, *AIChE J.* **9** (1963) 154.
[14] T. H. Chilton and A. P. Colburn, *Ind. Eng. Chem.* **26** (1934) 1183.
[15] R. B. Bird, W. E. Stewart, and E. N. Lightfoot, 'Transport phenomena', Wiley Int., New York (1960) p. 145.